LUND UNIVERSITY

Fluorescence spectra provide information on the depth of fluorescent lesions in tissue

Swartling, Johannes; Svensson, Jenny; Bengtsson, D; Terike, K; Andersson-Engels, Stefan

[Link to publication](#)

Fluorescence spectra provide information on the depth of fluorescent lesions in tissue

Johannes Swartling, Jenny Svensson, Daniel Bengtsson, Khaled Terike, and Stefan Andersson-Engels

The fluorescence spectrum measured from a fluorophore in tissue is affected by the absorption and scattering properties of the tissue, as well as by the measurement geometry. We analyze this effect with Monte Carlo simulations and by measurements on phantoms. The spectral changes can be used to estimate the depth of a fluorescent lesion embedded in the tissue by measurement of the fluorescence signal in different wavelength bands. By taking the ratio between the signals at two wavelengths, we show that it is possible to determine the depth of the lesion. Simulations were performed and validated by measurements on a phantom in the wavelength range 815–930 nm. The depth of a fluorescing layer could be determined with 0.6-mm accuracy down to at least a depth of 10 mm. Monte Carlo simulations were also performed for different tissue types of various composition. The results indicate that depth estimation of a lesion should be possible with 2–3-mm accuracy, with no assumptions made about the optical properties, for a wide range of tissues.   © 2005 Optical Society of America

OCIS codes: 170.3660, 170.3880, 170.6280, 170.7050.

1. Introduction

There is a rapidly growing interest in fluorescence measurements of embedded structures for tissue diagnostics. The principle is based on noninvasive or low-invasive techniques in which the tissue is irradiated with light and the remitted fluorescence signal is detected on the surface. The measured signal contains information about the concentration and distribution of the fluorophore. This type of measurement has the potential to discriminate diseased regions inside the tissue (e.g., tumors), provided that there is some mechanism for selective uptake of the fluorophore.

By use of long excitation wavelengths, approximately within the 600–900-nm range, it is possible to reach deep into the tissue, partly because of lower scattering, but mainly owing to the lower absorption in this region. A field of intense research is cancer diagnostics that uses fluorophores, which have long excitation wavelengths in the red or near-infrared (NIR) region. This would enable fluorescence emission from deep structures, of the order of several centimeters.[1,2] A specific application that has been suggested is detection of sentinel nodes in cancer patients.[3,4] Tumor spreading is routinely investigated by lymphoscintigraphy of the lymph nodes to which the lymphatic channels drain the tumor bed. A radioisotope is injected into the tumor volume, and the clinician searches for gamma decay in the nearby lymph nodes. Fluorescence-based detection could be a simpler and safer alternative to this procedure. Another application that has attracted interest is measurement of the fluorescence from photosensitizers for photodynamic therapy, with the aim of optimizing treatment parameters and monitoring photobleaching of the drug.[5,6]

Several reconstruction algorithms have been developed that attempt to recover the distribution of a fluorophore in a tissue volume given a set of measurements on the tissue surface. Fully three-dimensional reconstruction methods are being developed by some groups. They are commonly based on use of diffusion theory as the forward model,[7–11] but an algorithm based on the discrete-ordinates solution of the transport equation has also been proposed.[12] Many combinations of light source and detection points are needed for full reconstruction, which implies a high complexity of both the instrumentation and the reconstruction algorithm. A sim-

The authors are with the Department of Physics, Lund Institute of Technology, P.O. Box 118, SE-22100 Lund, Sweden. J. Swartling's e-mail address is js604@cam.ac.uk.

pler approach has been suggested by some authors, based on the approximation that the tissue can be regarded as a semi-infinite volume with fluorescing lesions at some depth beneath the surface. Stasic *et al.* presented a method based on the diffusion equation for a two-layer medium and spatially resolved measurements of both diffuse reflectance and fluorescence.[13] This method was successful in recovering the absorption and reduced scattering coefficients (μ_a and μ_s', respectively) of both layers, as well as the fluorophore concentration and layer depth. However, recovery of all parameters was limited to a depth of ∼3 mm, and determination of the depth itself proved to be difficult for larger depths owing to model coupling among depth, fluorophore concentration, and tissue absorption. Eidsath *et al.* have described a method based on image fluorometry.[4] Using a random-walk model, they demonstrated good accuracy of the determined depth for pointlike fluorescing lesions.

None of the methods described in the literature seem to make specific use of the spectral properties of the fluorescence signal. The measured emission spectrum following irradiation by excitation light at the surface is a function of several parameters, because the fluorescence light has to pass through tissue with characteristic scattering and absorption properties. Thus the intrinsic fluorescence emission spectrum will be altered in a way determined by the tissue optical properties, by the depth of the fluorophore, and also by the geometry of the light irradiation and the detection system. These effects have been noted by several authors in conjunction with fluorescence from shallow layers (less than ∼1 mm) and with ultraviolet or blue excitation light.[14–20]

In the first part of this paper we investigate the effects of the optical properties of the tissue and the measurement geometry on the recorded fluorescence spectra. We use Monte Carlo simulations to compute fluorescence spectra from a turbid medium. The Monte Carlo code was developed earlier and utilizes several techniques to reduce the number of photons necessary in the simulation to make the computation time reasonable even for entire fluorescence spectra and for large depths.[21] The computed spectra are compared with experimental results from a tissue phantom for different irradiation-detection geometries. The optical properties of the phantom, which are necessary for the simulations, are measured independently with an integrating sphere. The results serve as a validation of this method and demonstrate the effects on the measured fluorescence spectra.

Next we turn to the problem of determining the depth of fluorescent lesions in tissue. We recognize that the shape of the fluorescence spectrum from an embedded lesion is influenced by the depth of the lesion, owing to the fact that the fluorescence light is filtered when it migrates through the tissue to the surface. Thus we investigate the potential of using changes in the fluorescence spectra to estimate the depth, *d,* of a fluorescing lesion in a semi-infinite volume.

Our method relies on the fact that the absorption coefficient of the tissue is nonuniform over the spectral region of fluorescence emission. This means that relative spectral intensities change for different wavelength bands as the fluorescence light migrates to the surface. These changes can serve as a measure of the depth of the fluorophore. A simple approach is to form the ratio between the measured fluorescence signals at two wavelengths, λ_1 and λ_2,

$$\gamma = \frac{\Gamma(\lambda_1)}{\Gamma(\lambda_2)}, \qquad (1)$$

where Γ represents the probability of detecting a fluorescence photon and then evaluating the dependence of γ on d. An advantage of this approach is that by forming a ratio there is no need for absolute measurements of the fluorescence light, and some uncontrolled parameters cancel out. To prove the principle of this approach, we performed Monte Carlo simulations of excitation and fluorescence light. The simulation results were directly compared with the results from measurements performed on a tissue phantom to provide experimental verification of the method. We also performed a series of Monte Carlo simulations with realistic tissue optical properties, for various tissue types, to assess the robustness of the method with respect to biological variability.

2. Materials and Methods

A. Monte Carlo Simulations

The Monte Carlo method for simulating fluorescence from layered tissues has been described in depth in a previous study.[21] Briefly, our method takes advantage of the symmetry aspects to reduce the computation time. We also split the simulation of the excitation light and the emission light into two separate problems. The resulting data sets are convolved to provide the final answer. To increase the efficiency further, we apply a reciprocity theorem for the calculation of the emission light. This effectively reverses the photon paths of the fluorescence light so that only one simulation is needed, with the source of photons placed at the surface. It was shown that for certain applications, the computation time could be reduced by 2 orders of magnitude or more by use of these techniques, compared with the conventional method for simulating fluorescence.[21] The code is time resolved, which permits studies of the effects of fluorophore lifetimes and photon migration time dispersion.

For experimental validation, we performed Monte Carlo simulations with optical properties similar to those of phantoms, which were measured independently with an integrating-sphere method (Subsections 2.B–2.D below).

We also performed simulations with optical properties similar to those in real tissue. The absorption spectra for tissue were modeled based on data from previous measurements of breast tissue, in which the dominant absorbers in the red and NIR regions
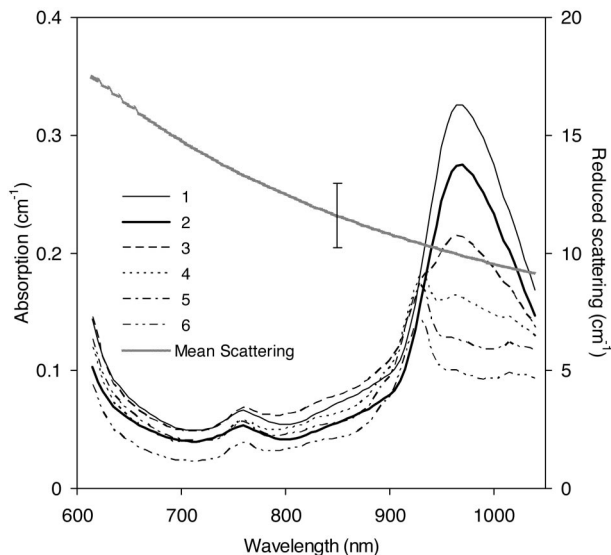
Fig. 1. Optical properties of six different types of breast tissue (from Pifferi *et al.*[22]). The absorption spectra represent fitted curves rather than actual measurement data. The reduced scattering spectra represent fits to a power law. Only the mean spectrum is shown for scattering to avoid cluttering in the graph. The error bar indicates the standard deviation.

Fig. 2. Schematic picture of the Intralipid phantom. The thickness of the fluorescing layer was 1 mm.

are water, fat, and deoxygenated and oxygenated hemoglobin.[22] The spectra of absorption and the reduced scattering that were used in the simulations are shown in Fig. 1. The tissue types ranged from water rich (62% water, 16% lipid for type 1) to lipid rich (12% water, 68% lipid for type 6) and thus represent a very wide span in terms of different tissue types.

B. Resin Phantom

We constructed a homogeneous solid phantom made of epoxy resin, following the guidelines in Ref. 23. We used TiO_2 particles at a concentration of 1 mg/g (T-8141; Sigma-Aldrich, St. Louis, Missouri) as a scatterer, and we used Amaranth dye at a concentration of 0.8 mg/g (12,056-1; Aldrich Chemical Company, St. Louis, Missouri) as an absorber. Small amounts of the Coumarin 30 dye were used to provide a fluorescence peak in the green region, 450–500 nm, and Sulforhodamin provided a peak in the red region, 550–650 nm, of the spectrum. The fluorescence spectrum of the phantom, following excitation at 407 nm, mimicked that of real tissue. It exhibited a broad peak in the green region that corresponded to tissue autofluorescence, and a red peak similar to the fluorescence from a fluorescent tumor marker.

C. Intralipid Phantom

To show the differences in the fluorescence spectrum for a lesion at different depths, we needed a phantom with an embedded inclusion at a variable depth *d*. To this end, a phantom was prepared from 1 part Intralipid-20% (Fresenius Kabi, Sweden) and 21 parts water. The phantom consisted of three layers, as depicted in Fig. 2. The upper and lower layers had
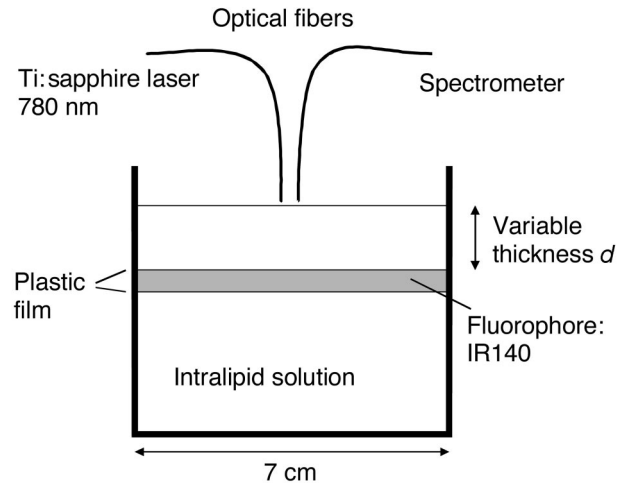
the same optical properties, and black ink was added to provide background absorption (2.3 μl/l). The middle layer, 1-mm thick, was separated by thin plastic foil, and to this layer a fluorescent dye (IR-140; Exciton, Dayton, Ohio) was added. The depth of the upper layer, *d,* could easily be varied by the addition or removal of the liquid.

D. Integrating Sphere Measurements

The optical properties of the phantoms were determined by use of an integrating sphere.[23] In the case of the solid phantom, a small amount of the resin was sandwiched between two glass slides while still not hardened. To measure the optical properties of the Intralipid phantom, we used a cuvette made of glass slides. In both cases the thickness of the samples was 1.00 mm and the lateral dimensions were 3 cm × 3 cm. The integrating-sphere setup was used to measure the total transmission, total reflectance, and collimated transmittance. In the case of the Intralipid phantom, the optical properties—μ_a, μ_s, and the scattering anisotropy factor *g*—were evaluated with Monte Carlo look-up tables.[23] For the solid phantom, the collimated measurement could not be performed because of high attenuation; instead, data for the *g* factor were taken from previous measurements on resin phantoms.[23] The data for the resin phantom were evaluated by use of the inverse adding–doubling method,[24] which was more convenient than the Monte Carlo look-up tables owing to the large differences in the optical properties at different wavelengths for this phantom.

E. Fluorescence Measurements

For the measurements on the resin phantom, we used a compact fluorescence point monitoring system to record the fluorescence spectra.[25] The fluorescence light from the sample was guided through a 600-μm-core-diameter step-index fiber (N.A. = 0.22) to a spectrometer and a cooled CCD camera (DH501-25U-01, Andor Technology, North-
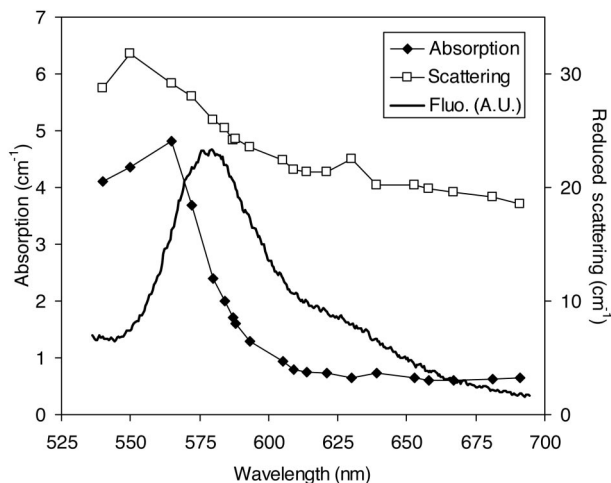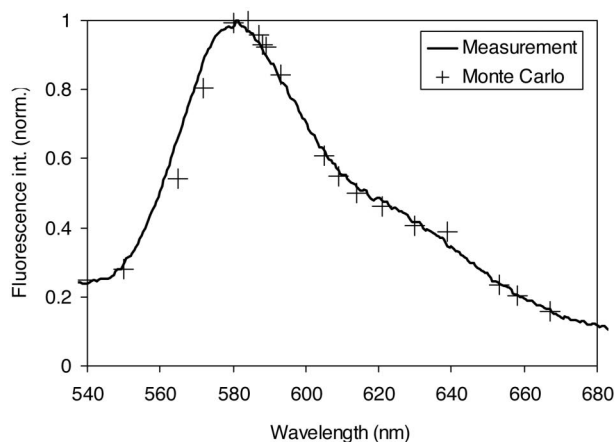
Fig. 3. Optical properties of the resin phantom measured with the integrating-sphere setup. Also shown is the intrinsic fluorescence spectrum (Fluo.) following excitation at 407 nm (arbitrary units).

ern Ireland). The tip of the fiber was in contact with the sample. For the excitation light source, we used a krypton-ion laser emitting at 407 nm with an output power of 20 mW. Light from the laser was focused on a 400-μm fiber, and the distal end of the fiber was imaged with a lens on the surface of the phantom. This 1:1 imaging arrangement gave a 400-μm top-hat excitation distribution on the surface. Fluorescence spectra were acquired for distances of 0.5–7 mm, in steps of 0.5 mm, from the excitation laser spot, over the spectral range 540–700 nm. The acquired fluorescence spectra were white-light calibrated and deconvolved from the spectral system response function.

We used a Ti:sapphire laser at 780 nm as the excitation source for the Intralipid phantom with a fluorescent layer. The power was limited to ∼10 mW. The light was guided to the phantom surface by a 400-μm-core-diameter step-index fiber (N.A. = 0.22), and a similar fiber collected the fluorescence light and guided it to a spectrometer (HoloSpec *f*/1.8*i*; Kaiser Optical Systems, Ann Arbor, Michigan). The laser wavelength was removed with a long-pass filter. A cooled CCD camera (LN/CCD-1024-EERB/1; Princeton Instruments, Trenton, New Jersey) was used for detection. Spectra were acquired over the spectral range 815–930 nm.
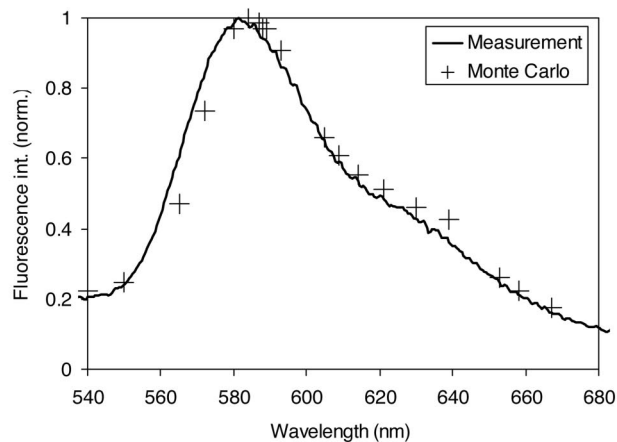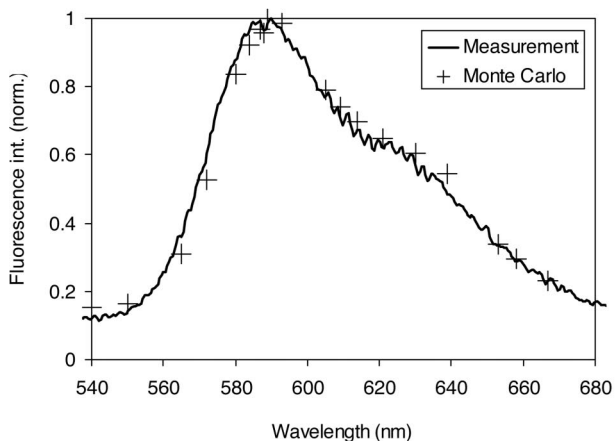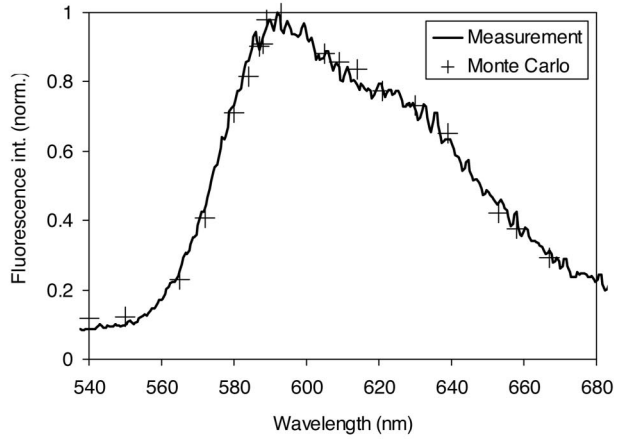

Fig. 4. Experimentally measured and calculated fluorescence spectra for the resin phantom. Results from different distances between the excitation spot and the detection fiber are shown: (a) 0.5 mm, (b) 1 mm, (c) 3 mm, and (d) 5 mm. Int., intensity; norm., normalized.
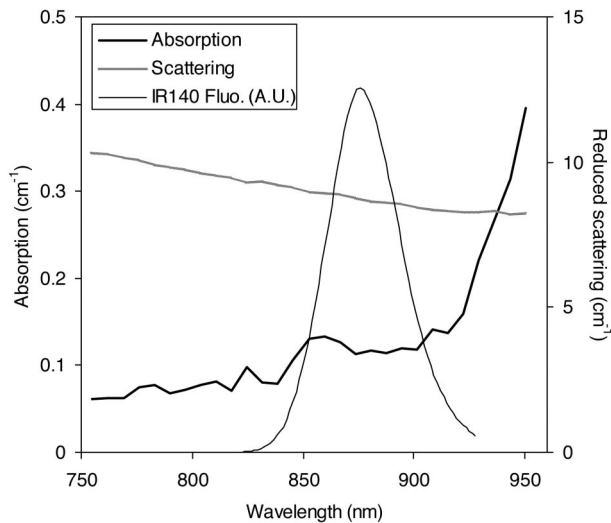
Fig. 5. Optical properties of the Intralipid phantom, as determined by the integrating-sphere setup. Also shown is the intrinsic fluorescence spectrum (Fluo.) of IR140 following excitation at 780 nm (arbitrary units).

3. Results

A. Resin Phantom and Monte Carlo Simulations

The optical properties of the resin phantom, as determined with the integrating-sphere system, are presented in Fig. 3, together with the intrinsic fluorescence spectra of the fluorophores. These data were subsequently used in the Monte Carlo simulations. The scattering anisotropy factor g was around 0.7 over the wavelength range.[23] The results of the simulations are presented in Fig. 4, together with the measurement results for the excitation wavelength of 407 nm. Four different fiber distances are shown: 0.5, 1, 3, and 5 mm. We observed a significant spectral shift as the fiber distance increased. Clearly, a good agreement between simulation and measurement was achieved.

B. Intralipid Phantom and Monte Carlo Simulations

The optical properties of the Intralipid phantom, as determined by the integrating-sphere method (shown in Fig. 5), were used as input for the Monte Carlo simulations. In this case g was around 0.65 over the wavelength range (data not shown). The measured fluorescence spectra at different depths are presented in Fig. 6, which shows the shift of the spectrum as the depth increases. In the Monte Carlo simulations the highest value of the ratio γ was obtained with λ_1 = 815 nm and λ_2 = 960 nm. However, owing to the low fluorescence signal at long wavelengths, we had to use a lower λ_2 to obtain a good signal-to-noise ratio from the measurements. Owing to the influence of autofluorescence when the excitation and detection fibers were close together, we used a fiber distance of 5 mm. Therefore the measurement was limited to depths larger than ~1 mm. In Fig. 7 we present γ (normalized to the value at d = 2 mm) as a function of d for λ_1 = 886 nm and λ_2 = 922 nm.
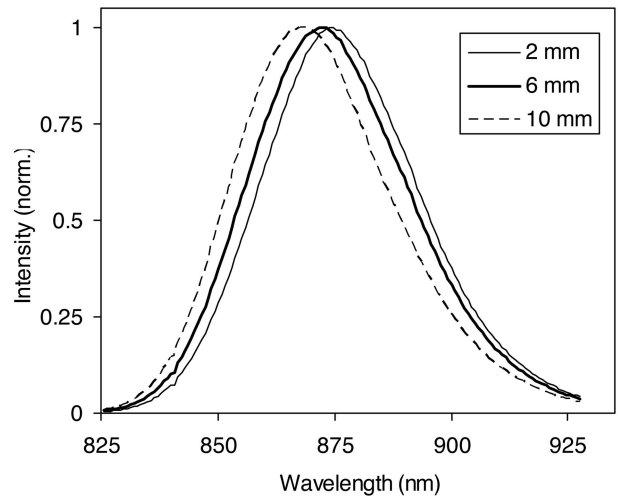

Fig. 6. Measured (normalized) fluorescence spectra for different layer depths (2, 6, and 10 mm) with fluorescing IR140.

By using the simulation results as a calibration curve, we also attempted to predict the depth of the fluorophore from the experimental values of γ. We then calculated the differences between the predicted and the true values of d, which resulted in a standard deviation in the predicted values of 0.6 mm.

C. Tissue Monte Carlo Simulations

For the simulations of realistic tissue, we assumed an excitation wavelength of 615 nm and simulated the fluorescence in the region 625–1005 nm in steps of 10 nm. For each individual simulation (i.e., one wavelength and one set of tissue optical properties), 5×10^5 photon histories were traced. The fluorescing lesion was simulated as a 1-mm-thick layer. The depth of the upper layer to the lesion was varied from 0 to 10 mm.
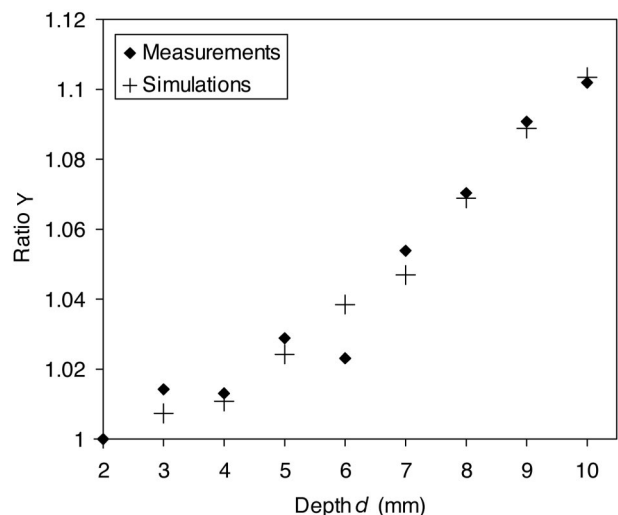

Fig. 7. Ratio γ shown for λ_1 = 886 nm and λ_2 = 922 nm as a function of the depth d, normalized to the value for d = 2. Results from both the Intralipid phantom measurements and the Monte Carlo simulations are shown.

The simulations were repeated for six different sets of tissue optical properties to account for typical biological variability of the tissue composition, as presented in Fig. 1. First, we wanted to investigate which ratios are the largest and thus best suited for evaluating the depth of the fluorophore. To determine the optimal choice of wavelengths for the method, we plotted $d\gamma/dd$ for 625 nm $< \lambda_1 <$ 1025 nm, 625 nm $< \lambda_2 <$ 1025 nm. Since the initial results showed that $\gamma(d)$ was approximately linear, we chose to plot $d\gamma/dd$ as determined by the slope of a regression line, rather than plotting $\gamma(d)$ for various depths. The results are presented in Figs. 8(a) and 8(b) for tissue types 1 and 6, respectively. The average of $d\gamma/dd$ for all six tissue types is shown in Fig. 8(c). The points with the largest values in these plots may be interpreted as corresponding to the best wavelength choices in terms of obtaining a high ratio.

By looking at $d\gamma/dd$, it is also possible to assess how robustly the ratios correspond to a given depth for different tissue types. We accomplished this by searching for the λ_1–λ_2 pair that gives the least variation in $d\gamma/dd$ among the six tissue types. With the requirement that we want $d\gamma/dd$ to be relatively high, the best combinations turned out to be λ_2 = 935 nm, with λ_1 = 695 nm, λ_1 = 745–755 nm, or λ_1 = 875 nm. At (λ_1, λ_2) = (695, 935 nm), the mean value was $d\gamma/dd$ = 0.063 mm^{-1}, with a standard deviation of 0.005 mm^{-1}. At (λ_1, λ_2) = (875, 935 mm), the mean value was $d\gamma/dd$ = 0.043 mm^{-1}, with a standard deviation of 0.005 mm^{-1}. We then applied these values to predict d from the simulation of each of the six tissue types. The result is shown in Fig. 9(a) for (λ_1, λ_2) = (695, 935 nm), and in Fig. 9(b) for (λ_1, λ_2) = (875, 935 nm). In the first case, most of the predicted values of d are within 1.5 mm of the true value, except for the most water-rich tissue type (1), which consistently overestimates the depth by approximately 2–2.5 mm. In the second case, the largest errors occur for tissue types 2 and 6, which are underestimated by as much as 2 mm.

4. Discussion

The results from the resin phantom (Fig. 4) clearly reveal that the shape of the recorded emission spectrum changes according to the detection geometry. As the distance between the source and the detector increases, more spectral intensity shifts to longer wavelengths where the absorption is lower. Similar findings have been reported by other authors.[16,18–20] The other important conclusion from the results of the resin phantom is that there is very good agreement between the Monte Carlo simulations and the measurements. Thus we are confident in the method of measuring the optical properties of the phantom independently by using the integrating sphere and then applying these values in the Monte Carlo simulations.

The results from the Monte Carlo simulations for a fluorescing layer show that the ratio $\gamma(\lambda_1, \lambda_2)$ is indeed a useful indicator of the depth of a fluorescing
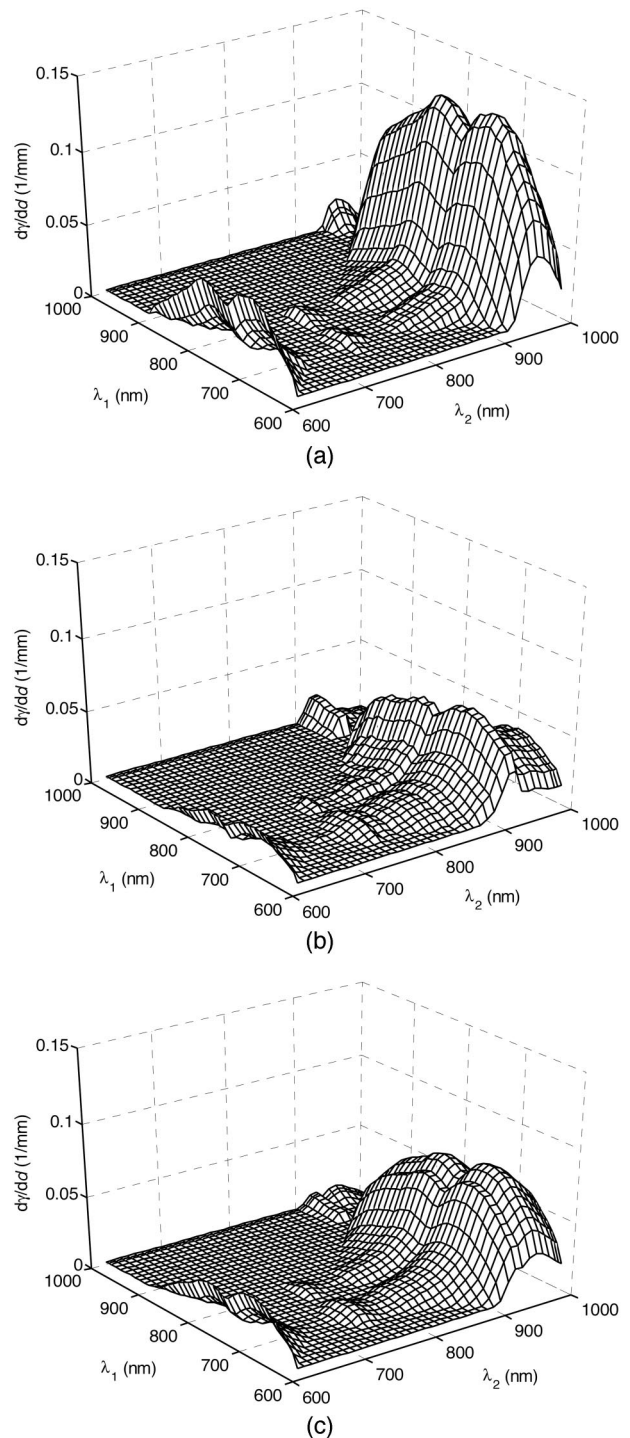

(a)

(b)

(c)

Fig. 8. Plots showing $d\gamma/dd$ as a function of λ_1 and λ_2. Only the values where $\gamma > 1$ are plotted. (a) Tissue type 1, water rich; (b) tissue type 6, lipid rich; (c) average of all six tissue types.

lesion for the right combinations of wavelengths λ_1 and λ_2. The results from the phantom measurements corroborate the simulations and show that the method is practically feasible with a relatively simple experimental setup. In the case of the Intralipid phantom, we utilize the difference in water absorption at the slope of the vibrational overtone band that
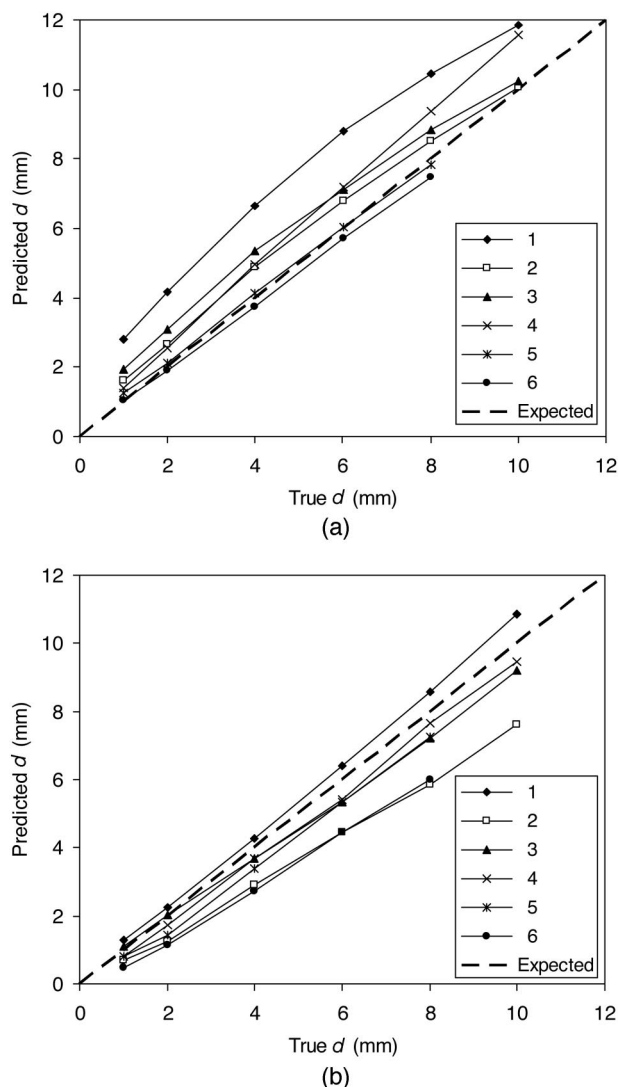
Fig. 9. Values of the depth d predicted from the Monte Carlo simulations for each of the six different tissue types. In all six cases the same calibration was used. (a) Calibration based on the mean value $d\gamma/dd = 0.063$ mm^{-1} at $(\lambda_1, \lambda_2) = (695, 935$ nm). (b) Calibration based on the mean value $d\gamma/dd = 0.043$ mm^{-1} at $(\lambda_1, \lambda_2) = (875, 935$ nm).

has a maximum absorption at 970 nm. Here we used $\lambda_2 = 922$ nm. Although a longer wavelength would have given a higher ratio γ, we were limited to $\sim$930 nm by the spectrometer and the fact that the fluorescence spectrum for IR140 drops to a low intensity for longer wavelengths (see Fig. 5). We were able to recover the depth of the fluorescing layer from the experimental data with an accuracy of 0.6 mm.

In real tissue there are two regions that may be of interest for choosing the wavelengths λ_1 and λ_2. One can either use the same slope of the water absorption band above 900 nm, as discussed above, or the slope of the hemoglobin absorption in the 600–650-nm region. The plot in Fig. 8(c) indicates that choosing λ_1 = 695 nm and $\lambda_2 = 975$ nm would be optimal. However, to get a robust estimate of the depth in a tissue in which the optical properties are unknown *a priori*,

the best choice is also governed by the requirement that γ be insensitive to biological variability. At $\sim$970 nm the water absorption band yields large differences between water-rich and lipid-rich tissue types, which means that there will be a large variation in $d\gamma/dd$ if $\lambda_2 = 975$ nm is chosen. Instead, using $\lambda_2 \approx 930$ is useful because this is a quasi-isosbestic point at which the variation between various soft tissues is minimal, owing to the fact that the absorption spectra of lipid and water cross at this wavelength.[22] Considering this, we found that the most robust combination of wavelengths was λ_1 = 695 nm and λ_2 = 935 nm. With this combination we could recover the depth of the layer with an error of less than 1.5 mm for all tissue types except the most water rich (type 1). Considering the very large differences in tissue composition and thus optical properties between the six tissue types, such a good prediction accuracy is quite encouraging. The use of the wavelength pair $(\lambda_1, \lambda_2) = (695, 935$ nm) may be problematic in practice, owing to difficulties in finding a suitable fluorophore with such a wide emission spectrum. Using the wavelengths $(\lambda_1, \lambda_2) = (875, 935$ nm) is a more realistic alternative, and the results in Fig. 9(b) show that the depth prediction accuracy for these wavelengths is similar.

It should also be noted that we found the relation between γ and d to be close to linear in all the cases we investigated, meaning that a single value of $d\gamma/dd$ is all that is needed to estimate the depth of a lesion for any measurement. However, the linear dependence of γ on d was only true when small distances between the excitation and the detection fibers were used. For distances above $\sim$5 mm, the relation deviated from linear when the depth was smaller than 1 or 2 mm. This could be of practical concern in some instances, since it may not be possible to place the excitation source and the detector close to each other because of the influence of autofluorescence in the tissue close to the excitation light source. In such cases it may be necessary to have a longer distance and to use nonlinear calibration curves.

It may be possible to improve the accuracy of the depth evaluation by incorporating methods to estimate the optical properties of the tissue, e.g., by measuring the diffuse white-light reflectance of the tissue. This would give some *a priori* information about the absorption and scattering properties in a manner related to the methods described by Stasic *et al.*[13] and Muller *et al.*[17]

We have also considered using temporal information to estimate the depth. The Monte Carlo simulations show that this may be possible, but there are several difficulties. Apart from the increased complexity in the instrumentation, decoupling the fluorophore lifetime and the photon migration time of flight is a nontrivial problem, especially since fluorophore lifetimes are typically an order of magnitude longer than the time of flight. The intrinsic fluorophore lifetime may change depending on the chemical environment, making this procedure increasingly difficult. For our method, we are analogously dependent on the

assumption that the intrinsic emission spectrum of the fluorophore does not change according to the chemical environment in the lesion. However, in our case such variations are likely to be small, whereas in the case of the lifetime it will be the dominating effect.

With the present method, we envision a potential application based on a probe that delivers excitation light and at the same time detects the fluorescence light by means of relatively simple photodetectors and wavelength-selecting filters. The operator would manually scan the probe across the tissue, and the information would be presented in the form of an indicator of fluorescence intensity and the estimated depth of the fluorophore. We also consider our method to be quite promising in terms of providing the depth information for image fluorometry and molecular imaging as a means for resolving the fluorophore distribution in three dimensions.[26]

References

1. V. Ntziachristos, J. Ripoll, and R. Weissleder, "Would near-infrared fluorescence signals propagate through large human organs for clinical studies?" Opt. Lett. **27,** 333–335 (2002).
2. V. Ntziachristos, C.-H. Tung, C. Bremer, and R. Weissleder, "Fluorescence molecular tomography resolves protease activity *in vivo,*" Nat. Med. **8,** 757–760 (2002).
3. J. S. Reynolds, T. L. Troy, R. H. Mayer, A. B. Thompson, D. J. Waters, K. K. Cornell, P. W. Snyder, and E. M. Sevick-Muraca, "Imaging of spontaneous canine mammary tumors using fluorescent contrast agents," Photochem. Photobiol. **70,** 87–94 (1999).
4. A. Eidsath, V. Chernomordik, A. H. Gandjbakhche, P. Smith, and A. Russo, "Three-dimensional localization of fluorescent masses deeply embedded in tissue," Phys. Med. Biol. **47,** 4079–4092 (2002).
5. T. J. Farrell, R. P. Hawkes, M. S. Patterson, and B. C. Wilson, "Modeling of photosensitizer fluorescence emission and photobleaching for photodynamic therapy dosimetry," Appl. Opt. **37,** 7168–7183 (1998).
6. T. Johansson, M. S. Thompson, M. Stenberg, C. af Klinteberg, S. Andersson-Engels, S. Svanberg, and K. Svanberg, "Feasibility study of a novel system for combined light dosimetry and interstitial photodynamic treatment of massive tumors," Appl. Opt. **41,** 1462–1468 (2002).
7. M. A. O'Leary, D. A. Boas, X. D. Li, B. Chance, and A. G. Yodh, "Fluorescence lifetime imaging in turbid media," Opt. Lett. **21,** 158–160 (1996).
8. D. Y. Paithankar, A. U. Chen, B. W. Pogue, M. S. Patterson, and E. M. Sevick-Muraca, "Imaging of fluorescent yield and lifetime from multiply scattered light reemitted from random media," Appl. Opt. **36,** 2260–2272 (1997).
9. J. Chang, H. L. Graber, and R. L. Barbour, "Imaging of fluorescence in highly scattering media," IEEE Trans. Biomed. Eng. **44,** 810–822 (1997).
10. M. J. Eppstein, D. J. Hawrysz, A. Godavarty, and E. M. Sevick-Muraca, "Three-dimensional, Bayesian image reconstruction from sparse and noisy data sets: near-infrared fluorescence tomography," Proc. Natl. Acad. Sci. USA **99,** 9619–9624 (2002).
11. A. B. Milstein, S. Oh, K. J. Webb, C. A. Bouman, Q. Zhang, D. A. Boas, and R. P. Millane, "Fluorescence optical diffusion tomography," Appl. Opt. **42,** 3081–3094 (2004).
12. A. D. Klose and A. H. Hielscher, "Fluorescence tomography with simulated data based on the equation of radiative transfer," Opt. Lett. **28,** 1019–1021 (2003).
13. D. Stasic, T. J. Farrell, and M. S. Patterson, "The use of spatially-resolved fluorescence and reflectance to determine interface depth in layered fluorophore distributions," Phys. Med. Biol. **48,** 3459–3474 (2003).
14. M. Keijzer, R. R. Richards-Kortum, S. L. Jacques, and M. S. Feld, "Fluorescence spectroscopy of turbid media: autofluorescence of the human aorta," Appl. Opt. **28,** 4286–4292 (1989).
15. S. Avrillier, E. Tinet, D. Ettori, J. M. Tualle, and B. Gélébart, "Influence of the emission-reception geometry in laser-induced fluorescence spectra from turbid media," Appl. Opt. **37,** 2781–2787 (1998).
16. C. Eker, "Optical characterization of tissue for medical diagnostics," Ph.D. dissertation (Lund Institute of Technology, Lund, Sweden, 1999).
17. M. G. Muller, I. Georgakoudi, Q. Zhang, J. Wu, and M. S. Feld, "Intrinsic fluorescence spectroscopy in turbid media: disentangling effects of scattering and absorption," Appl. Opt. **40,** 4633–4646 (2001).
18. Q. Liu, C. Zhu, and N. Ramanujam, "Experimental validation of Monte Carlo modeling of fluorescence in tissues in the UV-visible spectrum," J. Biomed. Opt. **8,** 223–236 (2003).
19. T. J. Pfefer, L. S. Matchette, A. M. Ross, and M. N. Ediger, "Selective detection of fluorophore layers in turbid media: the role of fiber-optic probe design," Opt. Lett. **28,** 120–122 (2003).
20. U. Utzinger and R. R. Richards-Kortum, "Fiber optic probes for biomedical optical spectroscopy," J. Biomed. Opt. **8,** 121–147 (2003).
21. J. Swartling, A. Pifferi, A. M. K. Enejder, and S. Andersson-Engels, "Accelerated Monte Carlo model to simulate fluorescence spectra from layered tissues," J. Opt. Soc. Am. A **20,** 714–727 (2003).
22. A. Pifferi, J. Swartling, E. Chikoidze, A. Torricelli, P. Taroni, A. Bassi, S. Andersson-Engels, and R. Cubeddu, "Spectroscopic time-resolved diffuse reflectance and transmittance measurements of the female breast at different interfiber distances," J. Biomed. Opt. **9,** 1143–1151 (2004).
23. J. Swartling, J. S. Dam, and S. Andersson-Engels, "Comparison of spatially and temporally resolved diffuse-reflectance measurement systems for determination of biomedical optical properties," Appl. Opt. **42,** 4612–4620 (2003).
24. S. A. Prahl, M. J. C. van Gemert, and A. J. Welch, "Determining the optical properties of turbid media by using the adding-doubling method," Appl. Opt. **32,** 559–568 (1993).
25. C. af Klinteberg, M. Andreasson, O. Sandström, S. Andersson-Engels, and S. Svanberg, "Compact medical fluorosensor for minimally invasive tissue characterisation," Rev. Sci. Instrum., submitted for publication.
26. C. Bremer, V. Ntziachristos, and R. Weissleder, "Optical-based molecular imaging: contrast agents and potential medical applications," Eur. J. Radiol. **13,** 231–243 (2003).